CORRELATING IMAGES AND RADAR AT PROMETHEI LINGULA IN THE SOUTH POLAR LAYERED DEPOSITS OF MARS. S. M. Milkovich, Jet Propulsion Laboratory, California Institute of Technology, M/S 230-205, 4800 Oak Grove Dr, Pasadena, CA 91109, USA. Sarah.M.Milkovich@jpl.nasa.gov

Introduction: The south polar layered deposits (SPLD) of Mars have been studied extensively for decades in images [e.g., 1-6]. The arrival of subsurface sounding radar such as SHARAD (SHallow RADar) onboard Mars Reconnaisance Orbiter allow us to see into the interior of the SPLD [7, 8]. Milkovich et al [9] demonstrated that a single SHARAD radar reflection can correspond to multiple layers at images of 6 m/pxl. By examining these layers in very high resolution HiRISE images (30 cm/pxl), we can look for patterns in the erosional styles of indicidual layers that may correlate with radar reflections.

This project is part of an ongoing effort to relate what is observed in images to what is observed by the radar with the goal of understanding the variations in physical properties between individual layers. This will in turn provide insights into the formation and history of these deposits.

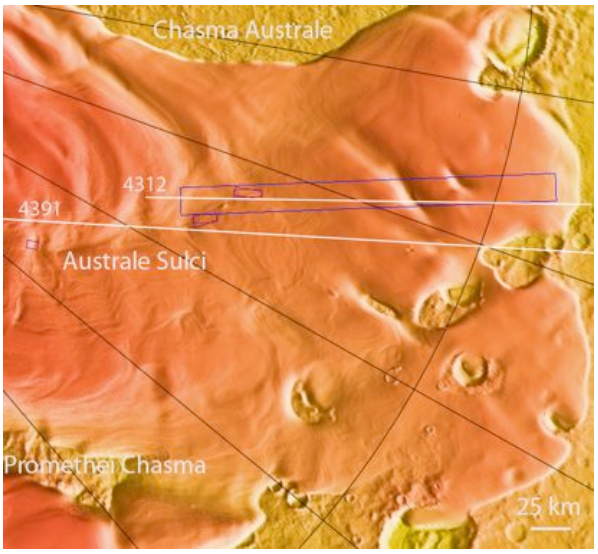

Fig. 1. Promethei Lingula. White lines indicate locations of SHARAD radargrams, blue box indicates locations of THEMIS images, purple boxes indicate locations of HiRISE images under study.

Radar and ice sheets: Radar-reflecting layers are observed in terrestrial ice sheets such as those in Antarctica and Greenland. Potential sources for these reflection include conductivity variations due to acidity changes, and variations in ice grain orientation [10]. Dusty layers in terrestrial ice sheets do correlate with some radar reflections, but this is due to the pH of the dust influencing the acidity, and thus the conductivity, of the ice [e.g., 11] rather than the amount or mineralogy of the dust changing the dielectric constant of the ice-dust mixture.

Lab experiments at 245 K [12] measure a real dielectric constant of 3.1-3.2 for pure ice, and ~ 3.4 for ice with 25% basaltic dust by mass fraction. Modelling by [13] of layered basaltic dust and ice indicates that dusty layers will cause reflections at SHARAD frequencies, and that a sequence of multiple dusty layers may cause a single radar reflection.

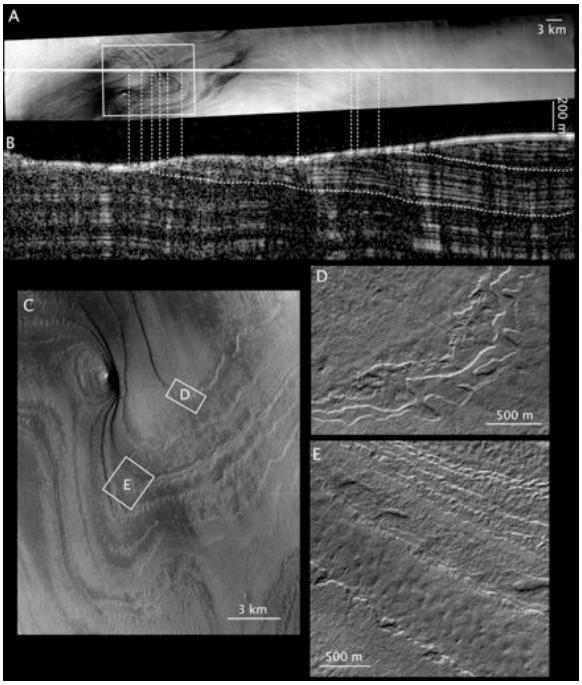

Fig 2. From [9]. A) THEMIS V08692012 B) SHARAD 4312. Dashed lines indicate correlating layers and reflections. C) subframe of V08692012 providing a closer look at the layers exposed on the surface. D) and E) subframes of R11/03432.

Promethei Lingula: The Promethei Lingula region is a lobe of the SPLD located approximately between 90˚E to 150˚E, where the SPLD extend into the Prometheus Basin [Fig. 1]. It is bounded by Chasma Australe on the west and Promethei Chasma on the east, and contains the canyon system Australe Sulci in its southern region, in which layers are exposed at the surface of the SPLD. Previous stratigraphic analysis of this area found evidence for multiple episodes of deposition separated by significant erosion in both images and radar [4, 5, 9].

Promethei Lingula is unusual within the SPLD due to the presence of many clear subsurface radar reflections directly below the surface [14].

Radar-Image comparisons: A number of the SHARAD radargrams in the Promethei Lingula region contain reflections that are truncated at the surface of the SPLD, allowing direct comparison between the layers exposed in images and the radar reflections. In a previous study, Milkovich et al [9] compared several radargrams with THEMIS 35 m/pxl images and found that layers in each image correlate with an individual reflection. Along SHARAD orbit 4312, they were also able to compare the radar reflections with a 6 m/pxl MOC image. They found that at higher resolution, what appears to be a single layer at THEMIS scales is actually multiple (3-7) layers eroding in groups, resulting in a stair-stepped topographic profile.

Since the analysis of [9], HiRISE has taken several images (see Fig. 1) of the surface of Promethei Lingula at very high (up to 30 cm/pxl) resolution.

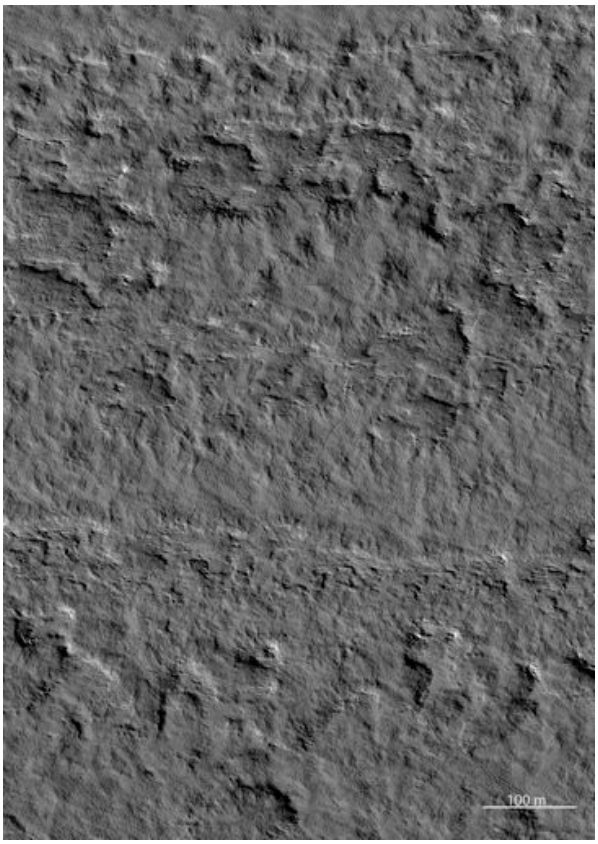

Fig 3: Subframe of HiRISE ESP_013714_0970.

Figure 3 shows a subframe of the HiRISE image ESP_013714_0970, located near V08692012. The 6 layers exposed within this subframe show great variety in erosional features, including the sinuosity of the eroded layer edge and the number and size of pits found on the surface of individual layers. This image has a corresponding image for a stereo pair, and the resulting anaglyph will aid this analysis. Additional radargrams in this area will also be studied for a more direct comparison.

Discussion: The underlying physical properties of the layers that cause their erosional behavior and surface textures may also cause a radar reflection. For example, a layer or group of layers that erode more easily than those above and below may have a higher dust to ice ratio and therefore a different dielectric response, resulting in a radar reflection. Further analysis of the detailed surface features of individual layers in HiRISE images can provide insight as patterns in erosional styles emerge.

Acknowledgments: Thanks to the SHARAD team for data assistance, and to K. E. Fishbaugh for image targeting assistance. This work was carried out at the Jet Propulsion Laboratory, California Institute of Technology, under a contract with the National Aeronautics and Space Administration.

References: [1] Murray, B.C. et al. (1972) *Icarus, 17*, 328-345. [2] Thomas, P. C. et al. (1992) in *Mars, ed. H. H. Kieffer et al.* pp. 767-798, Univ of AZ Press. [3] Malin, M. C. and Edgett, K. S. (2001) *JGR 106,* 23429-23570. [4] Kolb, E. J., and Tanaka, K. L. (2006) *Mars, 2,* 1-9. [5] Milkovich, S. M., Plaut, J. J. (2008) *JGR 113,* doi:10.1029/2007JE002987. [6] Herkenhoff, K. E. et. al. (2008) *LPSC 39*, 2361. [7] Seu, R. et al. (2004) *Planet Space Sci 52,* 157-166. [8] Seu, R. et al. (2007), *Science 317,* 1715-1718. [9] Milkovich, S. M. et al. (2009) *JGR 114*, doi:10.1029/2008JE003162. [10] Dowdeswell J. and Evans S. (2004) *Rep Prog Phys 67,* 1821-1861. [11] Eisen O., et al. (2003) *Tellus Ser B, 55*, 1007-1017. [12] Heggy et al (2007) *38th LPSC*, 1756, [13] Nunes D. C. and Phillips R. J. (2006) *JGR 111*, doi:10.1029/2005JE002609. [14] Phillips, R. et al. (2009) *40th LPSC*, 2007.